Materials Horizons

COMMUNICATION

View Article Online
View Journal



Cite this: DOI: 10.1039/c9mh01211g

Received 5th August 2019,
Accepted 22nd August 2019

DOI: 10.1039/c9mh01211g

rsc.li/materials-horizons



# Spatially modulated stiffness on hydrogels for soft and stretchable integrated electronics†

Hao Liu,[ab] Moxiao Li,[bc] Shaobao Liu,[abd] Pengpeng Jia,[ab] Xiaojin Guo,[be] Shangsheng Feng,[ab] Tian Jian Lu,[d] Huayuan Yang,[f] Fei Li *[ab] and Feng Xu *[ab]

**One major conundrum that impedes the development and application of emerging soft and stretchable electronics lies in the integration of electronic components with soft substrates for rational combination of various device functionalities into a single wearable state, since the rigid, nondeformable electronics tend to detach from the deformable substrate under mechanical loadings like stretch. Modulating the stiffness of soft materials in a spatially controllable manner provides a promising solution to this rigid–soft coupling challenge, by shielding the local strain of rigid components while maintaining the stretchable properties of the soft substrates. Hydrogels with superb biocompatibility and skin-like mechanical features are ideal candidates for interfacing the human body and electronic functionalities for cutting-edge wearable uses, where there exists a challenge of spatially modulating the stiffness of hydrogels to meet the application demands. Herein, we develop a facile and straightforward method to locally stiffen a hydrogel (with an increased Young's modulus of one order of magnitude) *via* an additional crosslinking strategy. The locally stiffened site undergoes minimal strain (down to 12%) and the untreated area remains stretchable under external deformations (100% strain), which presents excellent and tunable strain shielding capability to prevent detachment of the electronic components from the substrate under strain levels up to 150%. We further demonstrate a multifunctional health sensing device based on a component-integrated locally stiffened hydrogel and its satisfactory performance in monitoring temperature, UV exposure and EMG signals unveils its brilliant prospects for wearable healthcare applications.**

### New concepts

In this work, we proposed a local stiffening strategy through additional crosslinking on hydrogels for spatial modulation of hydrogel stiffness. This is a general method to manipulate the stiffness of hydrogel materials in a spatially programmable manner, and is the first time to realize integration of rigid electronic components with soft hydrogels for functional soft and stretchable electronics. Different from existing studies focusing on the modification of the bulky mechanical properties (*e.g.*, stiffness) of hydrogels as a whole, this study presented the concept of locally stiffened hydrogels where the stiffness on different areas of a hydrogel varies. Based on this result, integration of commercial electronic components for functional hydrogel electronics is achieved, offering a promising solution to the conundrum of coupling rigid electronic components with soft substrate materials. In addition, this is also the first time that multi-index monitoring of human health conditions with stretchable and biocompatible hydrogels has been realized. This research article offers a novel route for spatially controllable modulation of the mechanical properties of soft materials. And it is believed to be helpful for the fabrication of functional stretchable electronics with emerging biomaterials, especially aiming at the most advanced wearable healthcare applications where biocompatibility and mechanical coupling with the human body are highly appreciated.

## Introduction

Soft materials are usually elastically deformable under a certain range of mechanical loadings. Recent cutting-edge research advances have unfolded extensive interest in modulating the stiffness of soft materials (*e.g.*, plastics and hydrogels) to cater

[a] The Key Laboratory of Biomedical Information Engineering of Ministry of Education, School of Life Science and Technology, Xi'an Jiaotong University, Xi'an 710049, P. R. China. E-mail: feili@mail.xjtu.edu.cn, fengxu@mail.xjtu.edu.cn
[b] Bioinspired Engineering and Biomechanics Center (BEBC), Xi'an Jiaotong University, Xi'an 710049, P. R. China
[c] State Key Laboratory for Strength and Vibration of Mechanical Structures, Aerospace School, Xi'an Jiaotong University, Xi'an 710049, P. R. China
[d] State Key Laboratory of Mechanics and Control of Mechanical Structures, Nanjing University of Aeronautics and Astronautics, Nanjing 210016, P. R. China
[e] School of Science, Xi'an Jiaotong University, Xi'an 710049, P. R. China
[f] Department of Traditional Chinese Medicine Engineering, Shanghai University of Traditional Chinese Medicine, Shanghai 201203, P. R. China
† Electronic supplementary information (ESI) available. See DOI: 10.1039/c9mh01211g

for their diverse applications, including tissue engineering, soft actuating machines and soft and stretchable electronic devices.[1–4] For example, materials as tissue engineering matrices are generally required to be extremely soft (*i.e.*, ~kPa) with adaptable deformability to facilitate cell growth and differentiation, whereas those targeting at actuator uses are preferred to maintain higher stiffness (*i.e.*, ~MPa) to prevent fracture during repeating morphological and structural transformation.[5–8] As for substrates in the fabrication of soft and stretchable electronics, a trade-off analysis is expected to be conducted prior to material selection. In specific terms, softness and elasticity are highly appreciated for an ideal substrate to deform conforming to external stretch.[9–11] But, on the other hand, the stretchable feature of a soft substrate is unfriendly to the electronic components integrated on it, since these rigid and undeformed functional elements may suffer from detachment from the substrate under stretch, resulting in the function degradation of the whole device.[12,13]

To circumvent this paradox, a promising strategy is to spatially modulate the stiffness of the overall structure at the device level of stretchable electronics to reduce the local strain of components under stretch, while retaining the stretchability of the substrate at the same time. To date, various strain shielding approaches have been proposed to isolate rigid components from soft substrate deformation.[14–20] One popular approach is by introducing an adhesive layer or a rigid island bridging the electronic function layer and the supporting layer, to locally minimize the mechanical mismatch between the soft substrate and rigid components.[14–18] In this way, components mounted on rigid surfaces are protected from detachment even if large levels of strain are applied to the soft substrate, which consequently improves the functional stability and reliability of the stretchable electronic device. Apart from this solid-state scenario, other reports have revealed the feasibility of embedding electronic components inside the hollow structure of soft enclosure and filling the internal cavity with liquid (*e.g.*, silicone oligomer), to surround rigid components and absorb strains resulting from external deformations for component protection.[19,20] The liquid-filled enclosure demonstrates a remarkable strain-shielding effect, which allows for large substrate deformations with, however, negligible strain coupling to functional components. But this approach is associated with the potential issue of fluid leakage due to repeated mechanical loading, setting a potential drawback for its practical uses.

In spite of the great progress achieved in strain shielding for the design of soft and stretchable electronics, none of the abovementioned tactics turn out to be compatible with stiffness modulation on hydrogels. Hydrogels are nominated as favorable candidates as substrate materials for soft and stretchable electronics, owing to their advantages in terms of biocompatibility and skin-like stretchability.[21–25] These features are especially favorable for applications aiming at directly and conformably interfacing human physical/physiological indexes and electronic functionalities in a wearable manner. Although inserting glass slides as the intermediate island proves to be effective for bonding rigid elements onto a hydrogel substrate, the sharp and brittle glass poses an inevitable disadvantage for the stretchable electronic device itself and customers who incorporate it onto skin.[26] The liquid-based protocol may hardly work for a hydrogel either, because the internal porous structure can induce swelling of the hydrogel by absorbing the liquid from the aqueous environment. This phenomenon may further lead to loss of the strain-shielding liquid and uncontrollability over the morphology and electronic layout of hydrogel electronics. Thus, an effective stiffness modulation technique for local strain shielding on hydrogels is urgently demanded for integrating rigid electronic components onto hydrogel substrates and further realizing human-friendly, wearable and functional integrated hydrogel electronics.

In the present work, we develop a facile and straightforward scheme to spatially modulate hydrogel stiffness through local stiffening of the hydrogel. Locally stiffened patterns on a hydrogel featuring highly increased stiffness compared to that of the raw hydrogel can be easily achieved *via* additional crosslinking on the hydrogel. For example, the polyacrylamide-alginate (PAAm-alginate) hydrogel demonstrated here is locally stiffened through additional crosslinking with multivalent ions in specifically designed areas. The local stiffness of the hydrogel can be controllably adjusted by tuning the ion concentration and the time of additional ionic crosslinking, providing one order of magnitude enhancement of hydrogel stiffness. The locally stiffened hydrogel shows excellent strain shielding efficacy, with only ~12% actual strain observed in the stiffened area, relative to a 100% strain applied to the whole hydrogel substrate. With this strategy, rigid electronic components can be directly mounted onto the locally stiffened sites on the hydrogel to isolate strains induced by substrate stretch. We further develop a hydrogel-based multifunctional integrated electronic device for body-worn human health sensing to demonstrate its promising feasibility for advanced wearable healthcare applications.

## Results and discussion

Herein, a stretchable and tough PAAm-alginate hydrogel is taken as a representative example to demonstrate the spatial stiffness modulation on the hydrogel *via* additional crosslinking. The internal architecture of the PAAm-alginate hydrogel consists of an intertwined heat-polymerized PAAm network and an ion-crosslinked alginate network. It is known that crosslinking the alginate network with different multi-valent cations can result in notably variant mechanical properties of the hydrogel.[27] Based on this, it is possible to spatially modulate the stiffness of the hydrogel by locally crosslinking it with cations of different valences (Fig. 1a). In this study, the raw PAAm-alginate hydrogel is fabricated through successive procedures of heating the precursor solution in an oven and soaking it in $CaCl_2$ solution, to realize covalent crosslinking of PAAm and ionic crosslinking of alginate, respectively. The hydrogel is then locally stiffened by adding $FeCl_3$ solution to additionally crosslink the hydrogel in certain areas with the help of a patterned mold (Fig. S1, ESI†). During the additional crosslinking process, $Fe^{3+}$ ions replace the

 

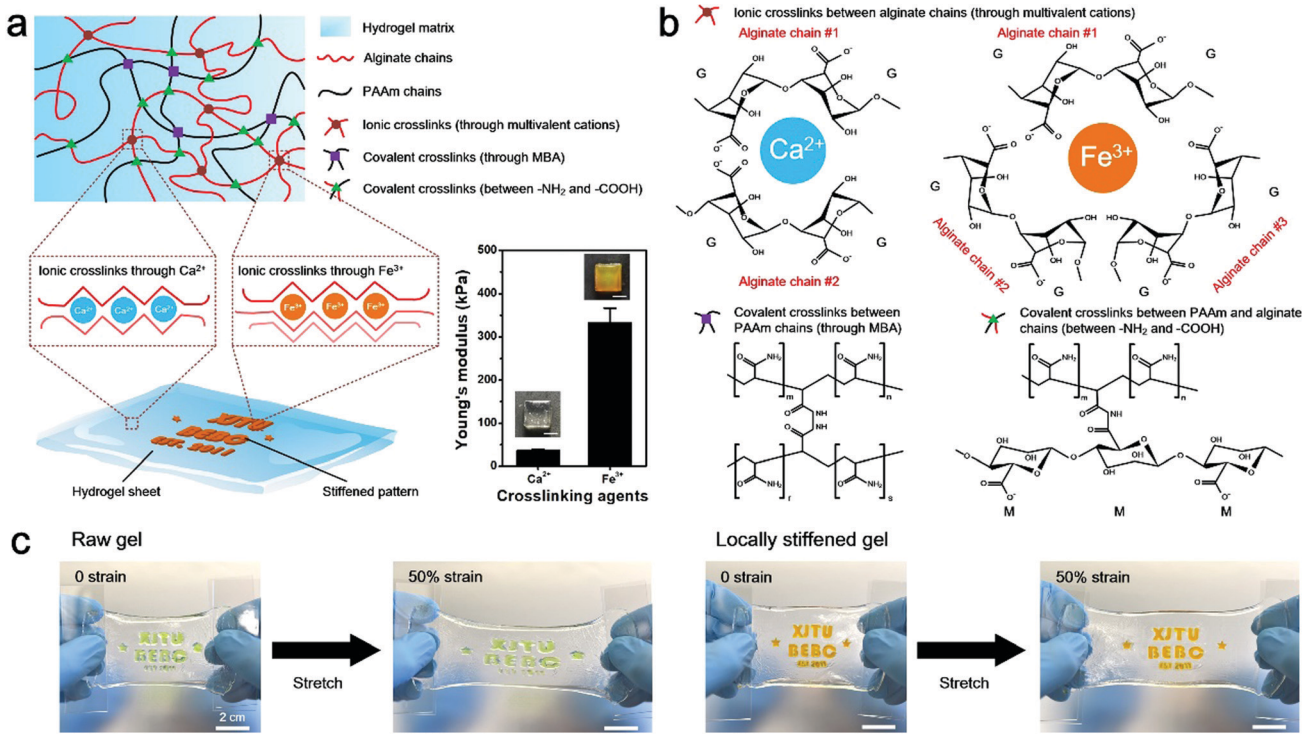


Fig. 1 Spatial modulation of hydrogel stiffness through local stiffening on a hydrogel. (a) Schematic illustration of the mechanism of local stiffening on the hydrogel *via* additional crosslinking with multi-valent cations. Right: Young's modulus of a $Ca^{2+}$ crosslinked hydrogel (raw hydrogel) and a $Fe^{3+}$ crosslinked hydrogel (stiffened hydrogel). Insets show photos of the two hydrogels. Scale bars: 1 cm. Error bars represent standard deviation ($N$ = 5). (b) Schematic of the chemical structure of PAAm-alginate hydrogels crosslinked with different multivalent cations. (c) Two hydrogel sheets with dyed (green food pigment) patterns and locally stiffened patterns in unstretched and stretched states to show the local strain shielding effect of the stiffened pattern.

$Ca^{2+}$ ions, forming trivalent ionic bonds to connect alginate chains (Fig. S2, ESI†). It is important to note that the trivalent-bonded hydrogel network (Young's modulus of ~330 kPa) is much stiffer than that merely consisting of chains connected through divalent bonds of $Ca^{2+}$ (Young's modulus of ~40 kPa), so the additionally $Fe^{3+}$-crosslinked area exhibits significantly enhanced stiffness on the whole piece of hydrogel (Fig. 1a and Fig. S3, ESI†). This phenomenon can be understood based on the different bonding modes of crosslinking the alginate hydrogel with $Ca^{2+}$ and $Fe^{3+}$. Divalent $Ca^{2+}$ links two alginate chains at the same time and crosslinks the hydrogel in a 2D planar manner. In comparison, trivalent $Fe^{3+}$ bonds three different alginate polymer chains together *via* interaction with carboxylic groups on each chain and establishes a 3D compact construct, leading to an improved mechanical stiffness of the hydrogel (Fig. 1b). In this way, the stiffened part of the hydrogel can be shielded from the strain of the overall hydrogel substrate, with minimal deformations compared to the obvious stretch of the raw, unstiffened areas on the hydrogel (Fig. 1c). As can be clearly seen from the experimental and simulation results shown in Fig. 2a, the strain of the stiffened central area (yellow) is far less than that of the unstiffened peripheral area (transparent). Underlying such a strain shielding effect is the fact that the unstiffened part of the hydrogel absorbs a majority of the strain applied to the stiffened section, as reflected by evidence that the actual strain on the unstiffened hydrogel even exceeds the total strain level of the overall hydrogel sheet (Fig. 2a).

Since the strain shielding effect is closely related to the stiffness of the locally modified area, it is of great importance to investigate the factors that determine the mechanics of the stiffened hydrogel. Experimental results in Fig. 2b exhibit that the stiffness of the hydrogel significantly increases over time of soaking in $FeCl_3$ solution for additional stiffening. A similar positive correlation can also be found between the stiffness and the $FeCl_3$ concentration in the range of 0.01–0.3 M. However, interestingly, the stiffness of the hydrogel witnesses a downward trend when the $FeCl_3$ concentration is higher than 0.3 M. This might be associated with the saturation of ionic crosslinking inside the alginate network at an $Fe^{3+}$ concentration level of 0.3 M, and when the $Fe^{3+}$ concentration exceeds 0.3 M, oversaturation may result in a structural heterogeneity and consequently a decreased stiffness of the hydrogel.[28] Since the stiffness of the hydrogel is dependent on the concentration of and soaking time in the $FeCl_3$ solution, it is understandable that the strain shielding effect can be tuned simply by varying these two parameters in a controllable manner (Fig. 2c and d). The tunable strain shielding efficacy can be validated by a local strain (of the stiffened area) spectrum ranging from 12% to 78% responding to the 100% total strain (of the whole hydrogel). This tunable phenomenon lies in the diffusion of

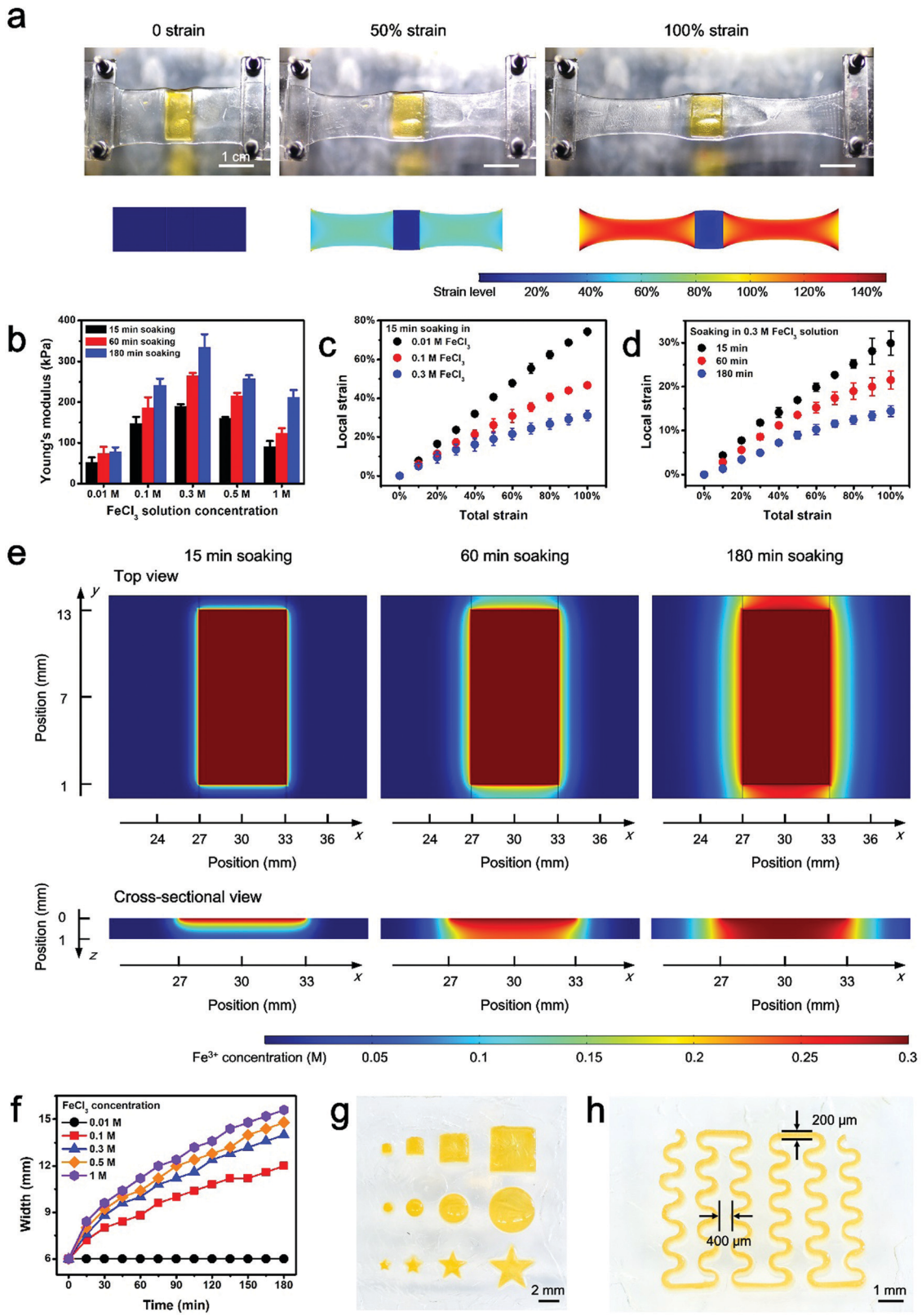


Fig. 2 Strain shielding effect of the locally stiffened hydrogel. (a) Digital photos and finite element analysis (FEA) results of the strain distribution of a locally stiffened (yellow rectangle pattern) hydrogel sheet under different levels of strain. (b) Young's modulus of the stiffened hydrogel *via* additional soaking in $FeCl_3$ solution as a function of solution concentration and soaking time. (c and d) Characterization results of the strain shielding effect of the locally stiffened hydrogel. The local strain of the stiffened area as a function of the total strain of the whole hydrogel with different $FeCl_3$ solution concentrations (c) and soaking times (d) for additional $Fe^{3+}$ crosslinking. Error bars represent standard deviation ($N = 5$). (e) FEA results of $Fe^{3+}$ ion diffusion in the hydrogel after 15, 60 and 180 min of soaking in $FeCl_3$ solution (0.3 M). (f) Simulation results on the width of the stiffened pattern as a function of time treated with $FeCl_3$ solutions of different concentrations. (g and h) Stiffened patterns of squares, circles, and stars in different sizes (g) and a serpentine line geometry on the hydrogel (h).

$Fe^{3+}$ ions throughout the hydrogel, where varying levels of $Fe^{3+}$ diffusion in planar and vertical directions are obtained simply by adjusting the two factors, namely the $FeCl_3$ solution concentration and soaking time in the $FeCl_3$ solution for local stiffening (Fig. 2e and Fig. S4 and S5, ESI†). Accordingly, such a variance leads to different extents of additional crosslinking of hydrogel networks with trivalent $Fe^{3+}$ ions, which form compact 3D architectures and enhanced interactions among the alginate chains to stiffen the hydrogel in a locally controllable mode. Note that $Fe^{3+}$ ions diffuse from the top to the bottom of the hydrogel, so the $Fe^{3+}$ ion concentration in the upper part of the hydrogel is greater than that in the lower region when the ion diffusion initializes. But the $Fe^{3+}$ ions diffuse quickly into the hydrogel. And as time goes on, their concentration distribution along the $z$ axis soon develops into a uniform state and the hydrogel in the depth profile can be uniformly crosslinked.

Additional attention is paid to the pattern-ability of this locally stiffening method, especially considering the expansion of patterns in size as a result of ion diffusion (Fig. 2f and Fig. S6, ESI†). Experimental results show that stiffened patterns with various shapes and sizes can be readily realized with the help of laser-etched molds (Fig. 2g). Furthermore, a minimum line width of 200 μm and a nearest inter-pattern distance of 400 μm can be achieved with the present molding technique (Fig. 2h), which reflects that the patterning resolution can be down to the sub-mm scale. Although the inevitably detrimental issue of planar ion diffusion resulting from the intrinsic stiffening mechanism may pose an adverse impact on the space between adjacent stiffened patterns (minimum of 400 μm, Fig. 2h) for component mounting and further hinder the miniaturization of electronic devices, it is capable of meeting the current criterion for commercial packaged electronic components whose pin–pin distance is normally 0.1 inch (2.54 mm). Besides, to assess the size effect on strain shielding, hydrogel substrates with locally stiffened circular patterns of various diameters (*i.e.*, 0.25, 1 and 2 mm) are put to the test. According to the data in Fig. S7 (ESI†), the strain shielding effects on samples with different sizes show negligible differences from each other, proving the universal adaptability of the proposed strategy to fabricate stiffened patterns on hydrogel with different geometries.

To examine the strain shielding effect for rigid component protection under stretch, the behavior of an operational amplifier chip, respectively, mounted on an untreated, raw hydrogel substrate and a locally stiffened hydrogel sheet is compared (Fig. 3a). Under 50% strain of the whole hydrogel, a noticeable chip detachment from the raw hydrogel substrate is observed. By contrast, the chip on the locally stiffened hydrogel is able to survive the 50% total strain and remains attached on the substrate, owing to the stiffened pattern which shields the local strain of the chip from the overall hydrogel deformation. In addition, an LED-integrated hydrogel circuit is uniaxially stretched to different strain levels to characterize its functional stability under mechanical loading (Fig. 3b). Different from that of the unstretched state, the LED on the raw hydrogel starts to detach from the substrate under 25% total strain and one LED pin even experiences complete detachment under 100% total strain, mainly due to the mechanical mismatch between the soft hydrogel and rigid LED pins. As a result, the LED fails to glow once the strain level of the whole device reaches 25%. However, as for the locally stiffened case where two separated circular patterns are stiffened on the hydrogel for the integration with LED pins, the LED maintains intact attachment to the substrate and no obvious function degradation of the hydrogel circuit is found even under a total strain of up to 150%. Numerical simulation analysis further explains the underlying mechanism for this phenomenon where the local strain of LED pins sharply decreases with the help of stiffened patterns and the component can be therefore protected from detachment under substrate stretch (Fig. 3c and Fig. S8, ESI†). More specifically, local strain of pins on the locally stiffened hydrogel under a total strain of 150% (Case #2) turns out to be even smaller than that of the same position on the untreated, raw hydrogel in response to 25% total strain (Case #1) (Fig. 3d). According to these comparison results, the reliable component protection efficacy through local stiffening of the hydrogel is clearly validated.

Targeting at cutting-edge wearable applications to provide insight into human health conditions, a multifunctional hydrogel sensor is demonstrated. The electronic sensing device is fabricated by integrating commercial electronic components onto a locally stiffened hydrogel substrate. It is composed of three functional modules, including the temperature sensing module, the ultraviolet (UV) sensing module and the electromyogram (EMG) sensing module (Fig. 4a). Details of circuit design and component selection are presented in Fig. S9 (ESI†). It should be worth noting that a thin layer of polydimethylsiloxane (PDMS) needs to be coated on component pins to avoid corrosion from the hydrogel, before components are integrated onto the locally stiffened hydrogel. The multifunctional hydrogel electronics presented here is a three-layer system consisting of (i) a bottom PAAm layer as the supporting substrate, (ii) a middle PAAm layer with patterned channels filled with liquid metal as conductive traces, and (iii) a top PAAm-alginate layer with locally stiffened patterns for integration with rigid components. In our design, tough bonding of the adjacent two hydrogel layers is important. Delamination of either hydrogel–hydrogel interface will cause irreversible damage to the hydrogel electronic device. Although the bonding between PAAm and PAAm-alginate has been previously studied and tough bridging of these hydrogels has been proved,[29,30] the bonding of the two PAAm layers remains a challenge. To overcome the weak bonding issue associated with the direct attachment of two PAAm hydrogels, a simple method of dispersing the PAAm precursor between the two hydrogel sheets prior to attaching is introduced. During the crosslinking of the additionally added PAAm by simply placing it at room temperature, PAAm molecules gradually diffuse into the two hydrogel layers and a tough bond between them is achieved *via* gluing of the intermediate PAAm when it is cured (Fig. S10a, ESI†). The tensile test results in Fig. S10b and c (ESI†) reveal significant enhancement in the adhesion strength and interfacial toughness of the PAAm–PAAm interface by adopting a PAAm precursor as the adhesive, compared to the direct attachment case. Also, the

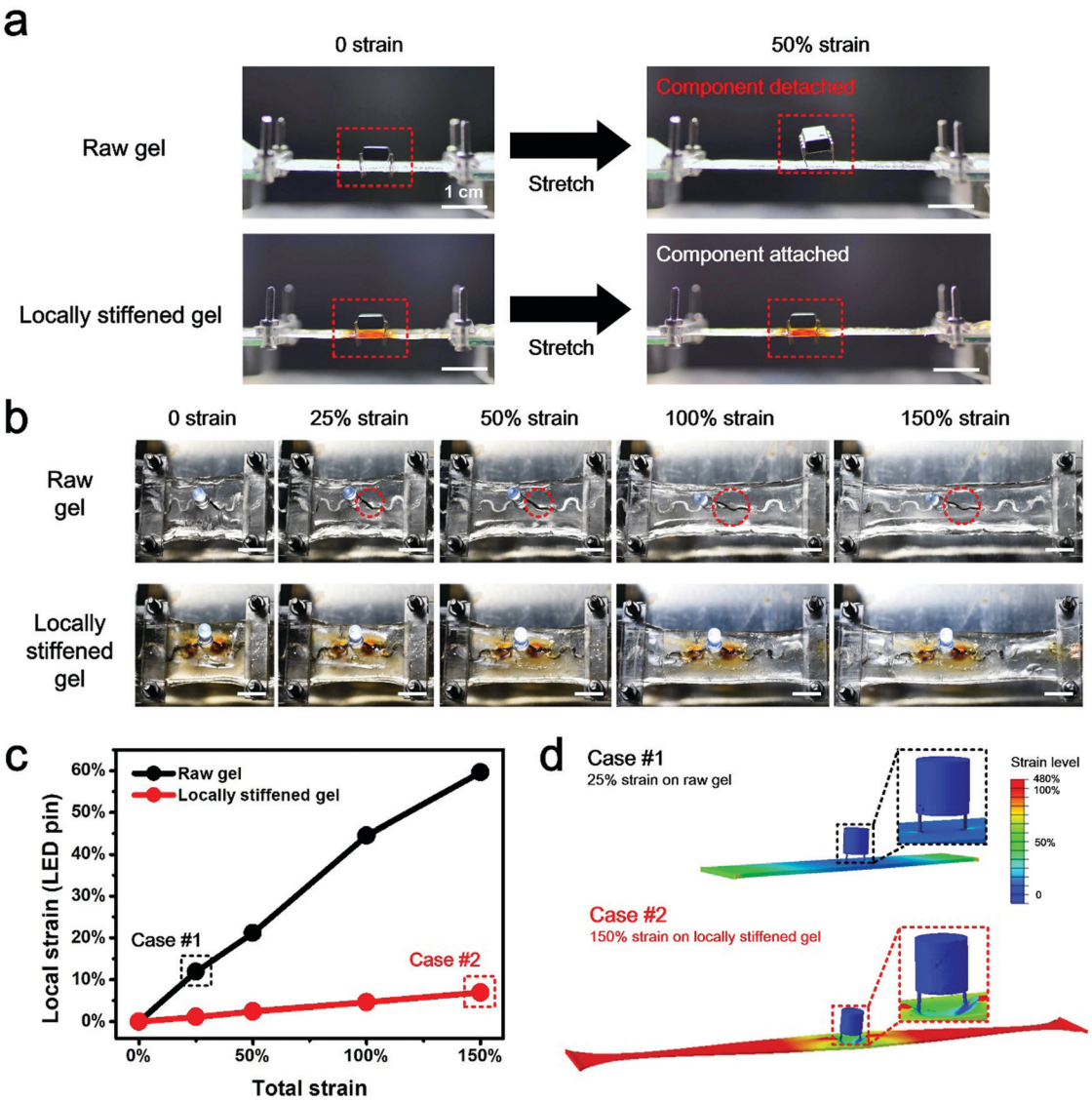


Fig. 3 Strain shielding of the locally stiffened hydrogel for electronic component integration and protection. (a) Digital photos of amplifier chip-integrated hydrogel devices under 0 and 50% total strain to demonstrate the ability of the locally stiffened hydrogel to protect components from detachment under stretch. Red dotted rectangles point out the rigid component mounted on the hydrogel. (b) Digital photos of LED-integrated hydrogel devices under different levels of total strain to demonstrate the ability of the locally stiffened hydrogel to promise the functional stability of the components under stretch. Note that two circular patterns are locally stiffened on the hydrogel for mounting of LED pins. Red dotted circles in the picture indicate the LED detachment from the raw hydrogel when the substrate is stretched, which causes dimming of the LED. Scale bars: 1 cm. (c) Numerical simulation results of the local strain of the LED pin-integrated position on the hydrogel under varying total strain levels. (d) Case studies of FEA results on comparison of the local strain of LED pins to demonstrate the strain shielding effect of the locally stiffened hydrogel for component protection under deformations.

bonding effect between the two PAAm hydrogels can be flexibly adjusted by using precursors relevant to hydrogels with different mechanical properties (Table S1, ESI†).

As can be seen from Fig. 4b, the fabricated hydrogel electronics can be incorporated onto human skin in a direct and conformable manner. Meanwhile, the excellent biocompatibility and skin-like mechanical features of hydrogels make the human–device interaction bio-friendly and the user experience of this wearable electronics is thus significantly improved. The hydrogel device integrated with functional electronic components and chips shows the capability to sustain a maximum strain of 50% at the device level, with no detachment of functional elements found (Fig. 4c). This component protection performance is attributed to the local stiffening effect, which shields the local strain at component-pinned sites on the locally stiffened hydrogel compared to its untreated counterpart, and accordingly avoids the component detachment and function degradation due to external strains (Fig. S11, ESI†). Although this tolerable strain level is much smaller than the maximum strain of a single-component integrated hydrogel device (*e.g.*, 150% strain for the LED-hydrogel electronics) because of the increased number and density for component integration, it is sufficient for on-skin uses.

 

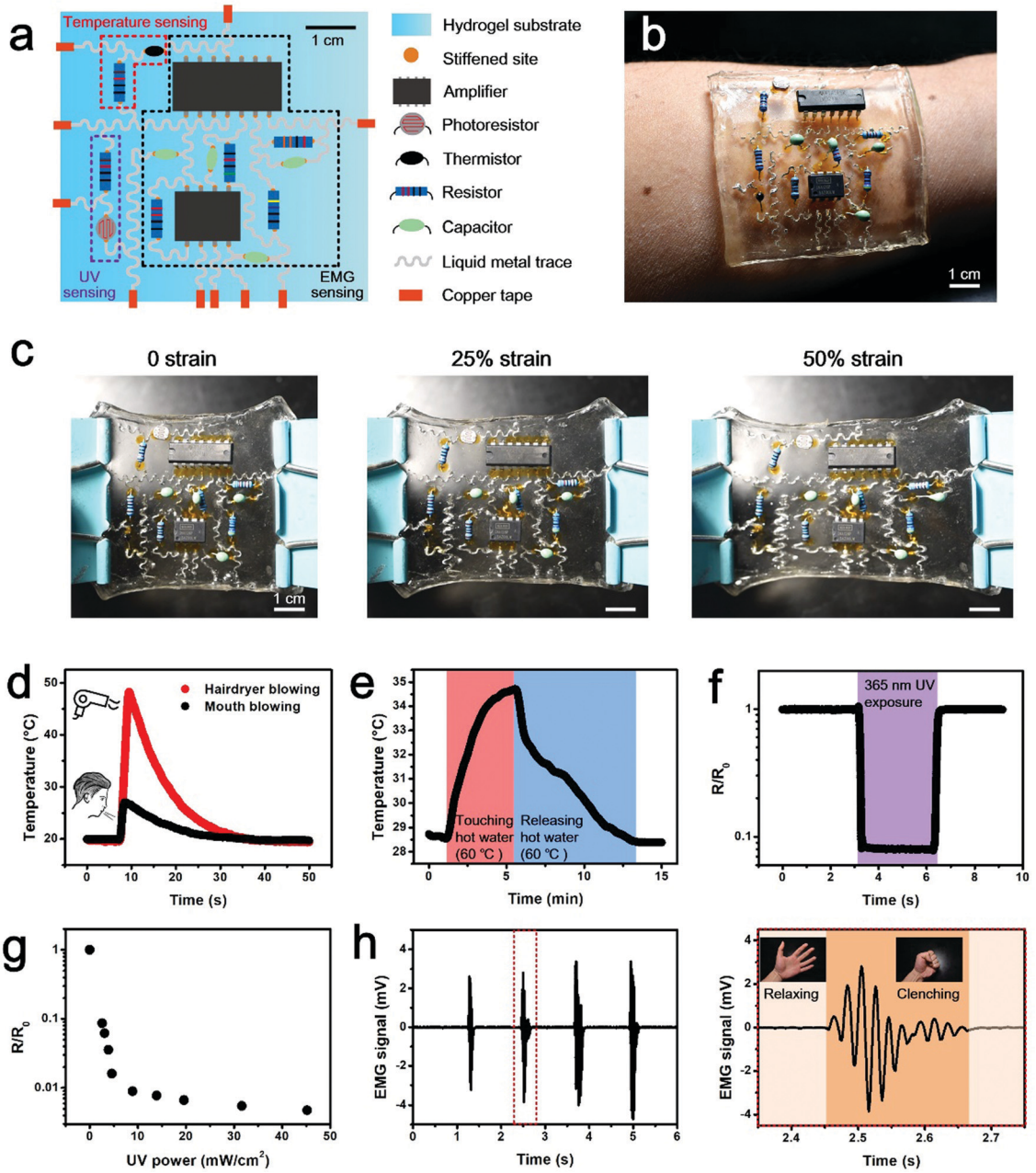


Fig. 4 Wearable, multifunctional integrated electronic sensing device based on locally stiffened hydrogels. (a) Design schematic of the hydrogel electronic device. (b) Digital photo of the fabricated hydrogel electronic device conformably attached on the skin of a human forearm. (c) Digital photos and the corresponding FEA results of integrated hydrogel electronics under different levels of strain. The structure at the device level is well maintained even under stretch, due to the local strain shielding of the locally stiffened hydrogel substrate. (d) Temperature signals acquired from directly blowing warm air through a hairdryer and a human mouth to the hydrogel device. (e) Temperature response of the skin to the hand touching and releasing a cup of hot water when the device is worn on the back of the hand. (f) Obvious variation of the output signal from the UV sensing module under UV exposure. (g) Output signal of the UV sensing module responding to different UV irradiation intensities. (h) EMG signals detected from repeated clenching and relaxing of the fist. Right: Enlarged view of the sensing data depicted by the red dotted rectangle in the left image.

Meanwhile, since no observable deformation can be found on pins of the component integrated on a locally stiffened hydrogel sheet under a strain level of 60%, it can be clarified that robust attachment of electronic components on the stretched hydrogel substrate is because of strain isolation deduced by local stiffening of the hydrogel, rather than the deformation of component pins, which conforms to the applied strain (Fig. S12, ESI†).

As for functional realization, temperature changes resulting from directly blowing warm air onto the hydrogel electronics with a hairdryer and mouth are displayed in Fig. 4d. The temperature sensing module shows quick response to the thermal stimulation and is able to distinguish the two different heating modes. Apart from the response to the direct thermal stimulation, the wearable hydrogel electronic device additionally

has an ability to sense the temperature variation of human skin as induced by hand grasping and releasing a cup of hot water (Fig. 4e). The signal read from the temperature sensing module increases when the hand is touching the hot water-containing cup and falls off when releasing it. Detection of UV intensity is important to avoid human sunburn, so the UV sensing ability is integrated into the device. Data obtained from the UV sensing module clearly indicates the exposure of UV (wavelength of 365 nm) irradiation leads to significant signal reduction (Fig. 4f), and the relationship between the sensing signal and UV power is established (Fig. 4g), which can be used to reflect the actual intensity of UV exposure. To provide data on human motion, the presented hydrogel electronics also shows the eligibility for EMG monitoring. As a demonstration, the EMG signal detected from the contraction and relaxation of the flexor carpi radialis muscle of the human forearm as a result of clenching and relaxing of the fist is presented in Fig. 4h and Video S1 (ESI†). According to the data, by using the integrated hydrogel electronics, it is feasible to acquire mV level signals with high signal to noise ratios, benefiting from the contribution of the amplification unit, the low-pass filtering unit and the high-pass filtering unit integrated within the hydrogel electronics. Despite the fact that body movements like fist clenching and relaxing cause deformation of skin where the wearable electronics is incorporated, the locally stiffened hydrogel substrate with spatially programmable stiffness can mitigate the local strain of integrated components and thus promises functional performance of the device. The wearable hydrogel device integrated with these three sensing functions provides users with insightful information about internal physiological situations and external natural environments, and is promising to witness application in outdoor sports training and indoor injury rehabilitation.

The major novelty of this work is adopting an additional crosslinking strategy to locally stiffen the hydrogel. It turns out to be able to modulate the stiffness of the hydrogel in a spatially programmable mode where the stiffness on different areas of hydrogel varies. Therefore, the stiffened part experiences minimal strain due to external deformations, while the untreated area remains stretchable. This design strategy offers an effective solution to the existing conundrum in the soft and stretchable electronics territory, namely coupling of rigid electronic components with soft substrate materials. Related evidence can be found in the satisfactory functional performance of component-integrated hydrogel electronics even under large levels of strain. In addition, employing hydrogel materials with bio-compatible features and similar-to-skin mechanical properties for multifunctional health sensing meets the development requirement of wearable healthcare purposes, promoting hydrogel electronics to undergo extensive applications in this emerging area.

Apart from these achievements, the present work could be further improved in the following aspects. To start with, the spatial resolution of local stiffening is primarily limited by the planar ion diffusion on the hydrogel substrate. Since the spatial resolution of patterning can be largely influenced by the ion diffusion process, a trade-off between patterning resolution and stiffening effects requires to be made when designing the paradigm for practical cases. Experimental parameters including the $FeCl_3$ concentration, treating time and hydrogel thickness can be well adjusted to cater for different requirements on spatial resolution and stiffening efficacy, under the guidance of simulation results presented in this work. On the other hand, even though the obtained outcome (minimum pattern–pattern distance of 400 μm) is compatible with the current package criteria for commercial electronic components (pin–pin distance of 2.54 mm), its competence to follow the miniaturization trend of electronic devices with higher component integration density remains a challenge. Surface mounted electronic components are of small size and light weight, so they are beneficial for propelling miniaturized electronics. While unlike the case for through-hole components that are pinned on the hydrogel, the entire component-covering area on the hydrogel should be stiffened to realize integration with surface mounted electronic components (Fig. S13, ESI†). Another promising way out may lie in photo-crosslinking of additive stiff hydrogel islands on the raw hydrogel substrate with the help of precisely-tailored photomasks. Because the fabrication precision of photomasks can be down to the micro-/nano-scale, the spatial resolution of stiffness modulation on hydrogels can be therefore improved for future miniaturized electronics.[31–33] Also, employing the advanced 3D printing technique for additionally patterning and crosslinking microgels on the raw hydrogel substrate may benefit improving the spatial resolution of local stiffening as well.[34,35]

Meanwhile, from the perspective of materials science, the local strain shielding effect for component protection can be further enhanced by increasing the stiffness of the additionally crosslinked hydrogel (with the Young's modulus reaching ~MPa).[36] Apart from stiffness, modulation of other mechanical parameters of hydrogels, including but not restricted to toughness, viscoelasticity and the fatigue limit, may also propel the research progress of hydrogel electronics. For instance, study on modulating the fatigue limit of hydrogels may provide guidelines to investigate the durability of hydrogel electronic devices, presenting a step closer to real-life applications. Additional attention should be paid to further improve user experience in a wireless way. Since wires connected to an outer circuit for power supply and signal transmission tend to get entangled with each other and cause inconvenience and discomfort when using, integrating a resonant radio frequency energy transfer module for power supply and near field communication chips for data delivery with the hydrogel electronics may help it to perform in a truly user-friendly manner.[37–39] Lastly, the device–skin interfacial adhesion is anticipated to be further enhanced with the adoption of novel biofriendly adhesives, establishing tough bonding interfaces between wearable electronics and human skin and thus improving the time-domain robustness of body-worn electronic devices, especially for long-term monitoring applications.[40,41]

## Conclusion

This study has proposed a simple method to spatially modulate the stiffness of a hydrogel through an additional crosslinking procedure to form locally stiffened patterns on the hydrogel.

 

Taking a PAAm-alginate hydrogel as an example, the stiffened hydrogel presents largely improved (one order of magnitude increased) mechanical stiffness, in contrast to the raw, untreated hydrogel. Therefore, these locally stiffened areas can shield the strain from intense deformation of the whole hydrogel substrate, and mounting rigid components onto these sites can protect them from detachment under stretch. Besides, the strain shielding effect of local stiffening can be well tuned by adjusting the crosslinking agent concentration and the time of the additional multi-valent ionic crosslinking. The tunable result shows that the local strain of the stiffened area can range from 12% to 78% responding to the 100% total strain of the whole hydrogel substrate, which is advantageous to meet different application demands. With the protection of locally stiffened patterns, a single component-integrated hydrogel electronic device is able to maintain the functionality under strain levels up to 150%, without component detachment and functional degradation. Finally, a multifunctional wearable sensing device based on integrating rigid, commercial electronic components onto a locally stiffened hydrogel is demonstrated. The excellent performance of this on-skin device in sensing temperature, UV exposure, and EMG signals has stimulated its promising application prospects for emerging human healthcare uses.

# Materials and methods

### Fabrication of a locally stiffened hydrogel

In the present study, polyacrylamide (PAAm)-alginate was selected as a model for fabricating a locally stiffened hydrogel. To initiate the preparation of a PAAm-alginate hydrogel, acrylamide (12.45 wt%), alginate (1.55 wt%), *N*,*N*′-methylenebisacrylamide (MBA, 0.0085 wt%) as the crosslinker and ammonium persulphate (APS, 0.025 wt%) as the thermal initiator were first dissolved in deionized water. The mixed solution then underwent a room-temperature degassing procedure in a vacuum environment for 15 min, before adding *N*,*N*,*N*′,*N*′-tetramethylethylenediamine (TEMED, 0.0775 wt%), the accelerator, to prepare a precursor solution of PAA-alginate. Subsequently, the precursor was poured onto a glass slide and successively put into an oven (70 °C, 1 hour) and soaked into 0.1 M $CaCl_2$ solution (room temperature, 15 min) to finally achieve a PAAm-alginate hydrogel. Local stiffening of the hydrogel was realized by covering a patterned polymethyl methacrylate (PMMA) mold on the surface of the hydrogel and then adding $FeCl_3$ solution to the hollow, patterned area. The patterned PMMA mold was designed and fabricated with a laser etcher (Universal VLS 2.30, USA). The concentration of the $FeCl_3$ solution was varied for different cases in this work. Due to the introduction of $Fe^{3+}$ which connects hydrogel chains *via* a trivalent ionic bond, the additional cation crosslinking step can locally stiffen the hydrogel in a spatially controllable manner (Fig. S1, ESI†).

### Tensile test of the raw hydrogel and the stiffened hydrogel

A tensile test of hydrogel samples was conducted with a tensile testing unit (ElectroForce® 3200 Series III, Bose, USA). Samples for the tensile test were uniformly molded into a dumbbell shape (length of 24 mm, thickness of 3 mm, width of 10 mm, gauge length of 4 mm and gauge width of 4 mm). Each sample was fixed to clamps of the tensile instrument and uniaxially stretched at a constant velocity (10 mm $min^{-1}$). The stress–strain data were recorded during performing the mechanical tensile test. Then the Young's modulus value was determined as the average slope over the 0–10% strain range of the stress–strain curve.

### Finite element analysis on the strain distribution of the locally stiffened hydrogel

Finite element simulation analyses were conducted using commercially available software (COMSOL Multiphysics 5.0, COMSOL, Sweden), to identify the strain distribution on the hydrogel under different strain loadings. The stretching process of the hydrogel electronics was simplified by a 2D linear elastic isotropy model due to slow diffusion under a relatively slow stretch process. The model consisted of a 36 mm × 12 mm rectangular soft substrate (Young's modulus: 30 kPa, density: 1.01 kg $m^{-3}$, Poisson ratio: 0.3) with a 7 mm × 12 mm rectangular stiffened region in the middle (Young's modulus: 300 kPa, density: 1.01 kg $m^{-3}$, Poisson ratio: 0.49).

### Finite element analysis on the strain distribution of a component-integrated hydrogel

Finite element simulations of an LED-integrated hydrogel were conducted using commercially available software (Abaqus 6.14, Dassault Systèmes, France). The model consisted of a 60 mm × 14 mm × 1 mm rectangular soft substrate (Young's modulus: 30 kPa, density: 1.01 kg $m^{-3}$, Poisson ratio: 0.33) with two 2 mm × 2 mm circular stiffened patterns (stiffened at pin-integrated sites) and a 7 mm × 12 mm elliptical stiffened region (stiffened in the whole component-covering area) in the middle (Young's modulus: 300 kPa, density: 1.01 kg $m^{-3}$, Poisson ratio: 0.49).

### Finite element analysis on ion diffusion

Finite element simulation analyses of the diffusion of $FeCl_3$ in the hydrogel were conducted using the transport of diluted species module of the commercially available software (COMSOL Multiphysics 5.3a, COMSOL, Sweden). A 3D geometric model for a 60 mm × 14 mm × 1 mm (length × width × thickness) hydrogel substrate was constructed. The diffusion process of $FeCl_3$ in the substrate can be described by the conservation equation:

$$\frac{\partial c}{\partial t} - \nabla \cdot (D \nabla c) = 0$$

where $D$ is the diffusion coefficient of $FeCl_3$ in the hydrogel, and it is set as $2 \times 10^{-10}$ $m^2$ $s^{-1}$.

The $FeCl_3$ concentration is assumed to be constant in the stiffened region and it is set as 0.01 M, 0.1 M, 0.3 M, 0.5 M and 1 M, respectively. The initial concentration of $FeCl_3$ is 0 in the substrate, and there is no flux at the other walls. As for characterization of diffusion-induced size expansion, only the area where the $Fe^{3+}$ concentration exceeds the threshold value of 0.005 M is regarded effective.

### Fabrication of hydrogel electronics

A precursor solution for a PAAm hydrogel was prepared according to Table S1 (ESI†). The bottom PAAm layer was room-temperature crosslinked on a flat glass slide, while the middle PAAm layer was crosslinked in a serpentine-patterned PMMA mold to form channels on it. Prior to attaching these two layers, 100 μL PAAm precursor solution (30 kPa, Table S1, ESI†) was pipetted onto the interface to form tough interfacial bonding and copper tapes were placed at the terminals of the patterned channels between them as electrodes to connect with the outer circuit. Afterwards, liquid metal (Eutectic Gallium Indium, Sigma Aldrich, USA) was syringe-injected into embedded channels. In the next step, a thin layer of the PAAm-alginate hydrogel was formed on the top and local stiffening on it was realized by additional cationic crosslinking with 0.3 M $FeCl_3$ solution for 15 min. The total dimensions of the three-layer hydrogel for the LED-integrated device are: length – 30 mm, width – 20 mm, and thickness – 3 mm. The dimensions of the three-layer hydrogel for the multifunctional integrated device are: length – 66 mm, width – 58 mm, and thickness – 3 mm. The size of the locally stiffened pattern for component pin mounting is 2 mm in diameter. A thin layer of polydimethylsiloxane (PDMS) was then coated on component pins before integrating electronic components onto the hydrogel.

### Demonstration of the multifunctional hydrogel sensing electronics

Details about the design and placement on the human body of the multifunctional hydrogel sensing electronics are illustrated in Fig. S4 (ESI†). Temperature sensing was carried out under conditions of a hairdryer blowing warm air, a mouth blowing warm air, and a hand touching and releasing a cup of hot water. UV sensing was conducted by exposing the hydrogel electronics to 365 nm UV light from a UV crosslinker (S2000-XLA, OmniCure, USA) in a dark room. EMG sensing was realized through repeated clenching and relaxing of a fist. Sensing data were wire-transmitted to and displayed on a multi-channel oscilloscope (UTD2102CM, UNI-T, China). A dual-channel DC power supply (ZF-303D, Zhaoxin, China) provided electric power to the hydrogel electronic device. All the demonstrations were performed by the first author with informed consent.

## Conflicts of interest

There are no conflicts to declare.

## Acknowledgements

This work was financially supported by the National Natural Science Foundation of China (21775117), the General Financial Grant from the China Postdoctoral Science Foundation (2016M592773), the High Level Returned Overseas Students Foundation ([2018]642), the Key Program for Science and Technology Innovative Research Team in Shaanxi Province of China (2017KCT-22), the National Key Research and Development Program of China (2018YFC1707702) and the Fundamental Research Funds for the Central Universities (PY3A081, xjh012019044).

## References

1 J.-Y. Sun, X. Zhao, W. R. K. Illeperuma, O. Chaudhuri, K. H. Oh, D. J. Mooney, J. J. Vlassak and Z. Suo, *Nature*, 2012, **489**, 133–136.
2 C. Yang, M. W. Tibbitt, L. Basta and K. S. Anseth, *Nat. Mater.*, 2014, **13**, 645.
3 E. Ducrot, Y. Chen, M. Bulters, R. P. Sijbesma and C. Creton, *Science*, 2014, **344**, 186.
4 X. Zhao, *Proc. Natl. Acad. Sci. U. S. A.*, 2017, **114**, 8138.
5 G. Huang, F. Li, X. Zhao, Y. Ma, Y. Li, M. Lin, G. Jin, T. J. Lu, G. M. Genin and F. Xu, *Chem. Rev.*, 2017, **117**, 12764–12850.
6 B. E. de Avila, P. Angsantikul, J. Li, M. Angel Lopez-Ramirez, D. E. Ramirez-Herrera, S. Thamphiwatana, C. Chen, J. Delezuk, R. Samakapiruk, V. Ramez, L. Zhang and J. Wang, *Nat. Commun.*, 2017, **8**, 272.
7 Y. Li, C. T. Poon, M. Li, T. J. Lu, B. Pingguan-Murphy and F. Xu, *Adv. Funct. Mater.*, 2015, **25**, 5999–6008.
8 R. F. Shepherd, F. Ilievski, W. Choi, S. A. Morin, A. A. Stokes, A. D. Mazzeo, X. Chen, M. Wang and G. M. Whitesides, *Proc. Natl. Acad. Sci. U. S. A.*, 2011, **108**, 20400.
9 D.-H. Kim, N. Lu, R. Ma, Y.-S. Kim, R.-H. Kim, S. Wang, J. Wu, S. M. Won, H. Tao, A. Islam, K. J. Yu, T.-I. Kim, R. Chowdhury, M. Ying, L. Xu, M. Li, H.-J. Chung, H. Keum, M. McCormick, P. Liu, Y.-W. Zhang, F. G. Omenetto, Y. Huang, T. Coleman and J. A. Rogers, *Science*, 2011, **333**, 838–843.
10 C. Larson, B. Peele, S. Li, S. Robinson, M. Totaro, L. Beccai, B. Mazzolai and R. Shepherd, *Science*, 2016, **351**, 1071–1074.
11 N. Matsuhisa, M. Kaltenbrunner, T. Yokota, H. Jinno, K. Kuribara, T. Sekitani and T. Someya, *Nat. Commun.*, 2015, **6**, 7461.
12 K. I. Jang, K. Li, H. U. Chung, S. Xu, H. N. Jung, Y. Yang, J. W. Kwak, H. H. Jung, J. Song, C. Yang, A. Wang, Z. Liu, J. Y. Lee, B. H. Kim, J. H. Kim, J. Lee, Y. Yu, B. J. Kim, H. Jang, K. J. Yu, J. Kim, J. W. Lee, J. W. Jeong, Y. M. Song, Y. Huang, Y. Zhang and J. A. Rogers, *Nat. Commun.*, 2017, **8**, 15894.
13 Y. Khan, M. Garg, Q. Gui, M. Schadt, A. Gaikwad, D. Han, N. A. D. Yamamoto, P. Hart, R. Welte, W. Wilson, S. Czarnecki, M. Poliks, Z. Jin, K. Ghose, F. Egitto, J. Turner and A. C. Arias, *Adv. Funct. Mater.*, 2016, **26**, 8764–8775.
14 J. Wu, M. Li, W.-Q. Chen, D.-H. Kim, Y.-S. Kim, Y.-G. Huang, K.-C. Hwang, Z. Kang and J. A. Rogers, *Acta Mech. Sin.*, 2010, **26**, 881–888.
15 D.-H. Kim, Y.-S. Kim, J. Wu, Z. Liu, J. Song, H.-S. Kim, Y. Y. Huang, K.-C. Hwang and J. A. Rogers, *Adv. Mater.*, 2009, **21**, 3703–3707.
16 S. Wagner and S. Bauer, *MRS Bull.*, 2012, **37**, 207–213.
17 Y. Wang, C. Zhu, R. Pfattner, H. Yan, L. Jin, S. Chen, F. Molina-Lopez, F. Lissel, J. Liu, N. I. Rabiah, Z. Chen, J. W. Chung, C. Linder, M. F. Toney, B. Murmann and Z. Bao, *Sci. Adv.*, 2017, **3**, e1602076.
18 J. Lee, J. Wu, J. H. Ryu, Z. Liu, M. Meitl, Y. W. Zhang, Y. Huang and J. A. Rogers, *Small*, 2012, **8**, 1851–1856.

 

19 S. Xu, Y. Zhang, L. Jia, K. E. Mathewson, K.-I. Jang, J. Kim, H. Fu, X. Huang, P. Chava, R. Wang, S. Bhole, L. Wang, Y. J. Na, Y. Guan, M. Flavin, Z. Han, Y. Huang and J. A. Rogers, *Science*, 2014, **344**, 70.
20 Y. Ma, M. Pharr, L. Wang, J. Kim, Y. Liu, Y. Xue, R. Ning, X. Wang, H. U. Chung, X. Feng, J. A. Rogers and Y. Huang, *Small*, 2017, **13**, 1602954.
21 S. Zhao, P. Tseng, J. Grasman, Y. Wang, W. Li, B. Napier, B. Yavuz, Y. Chen, L. Howell, J. Rincon, F. G. Omenetto and D. L. Kaplan, *Adv. Mater.*, 2018, **30**, e1800598.
22 D. Wirthl, R. Pichler, M. Drack, G. Kettlguber, R. Moser, R. Gerstmayr, F. Hartmann, E. Bradt, R. Kaltseis, C. M. Siket, S. E. Schausberger, S. Hild, S. Bauer and M. Kaltenbrunner, *Sci. Adv.*, 2017, **3**, e1700053.
23 H. Liu, M. Li, C. Ouyang, T. J. Lu, F. Li and F. Xu, *Small*, 2018, **14**, e1801711.
24 J. Y. Sun, C. Keplinger, G. M. Whitesides and Z. Suo, *Adv. Mater.*, 2014, **26**, 7608–7614.
25 C. Yang and Z. Suo, *Nat. Rev. Mater.*, 2018, **3**, 125–142.
26 S. Lin, H. Yuk, T. Zhang, G. A. Parada, H. Koo, C. Yu and X. Zhao, *Adv. Mater.*, 2016, **28**, 4497–4505.
27 C. H. Yang, M. X. Wang, H. Haider, J. H. Yang, J.-Y. Sun, Y. M. Chen, J. Zhou and Z. Suo, *ACS Appl. Mater. Interfaces*, 2013, **5**, 10418–10422.
28 C. K. Kuo and P. X. Ma, *Biomaterials*, 2001, **22**, 511–521.
29 J. Li, A. D. Celiz, J. Yang, Q. Yang, I. Wamala, W. Whyte, B. R. Seo, N. V. Vasilyev, J. J. Vlassak, Z. Suo and D. J. Mooney, *Science*, 2017, **357**, 378.
30 H. Yuk, T. Zhang, S. Lin, G. A. Parada and X. Zhao, *Nat. Mater.*, 2015, **15**, 190.
31 B. J. Klotz, D. Gawlitta, A. J. W. P. Rosenberg, J. Malda and F. P. W. Melchels, *Trends Biotechnol.*, 2016, **34**, 394–407.
32 K. Yue, G. Trujillo-deSantiago, M. M. Alvarez, A. Tamayol, N. Annabi and A. Khademhosseini, *Biomaterials*, 2015, **73**, 254–271.
33 U. A. Gurkan, Y. Fan, F. Xu, B. Erkmen, E. S. Urkac, G. Parlakgul, J. Bernstein, W. Xing, E. S. Boyden and U. Demirci, *Adv. Mater.*, 2013, **25**, 1192–1198.
34 K. Tian, J. Bae, S. E. Bakarich, C. Yang, R. D. Gately, G. M. Spinks, M. In Het Panhuis, Z. Suo and J. J. Vlassak, *Adv. Mater.*, 2017, **29**, 1604827.
35 A. Sydney Gladman, E. A. Matsumoto, R. G. Nuzzo, L. Mahadevan and J. A. Lewis, *Nat. Mater.*, 2016, **15**, 413.
36 J. Li, W. R. K. Illeperuma, Z. Suo and J. J. Vlassak, *ACS Macro Lett.*, 2014, **3**, 520–523.
37 J. Koo, M. R. MacEwan, S.-K. Kang, S. M. Won, M. Stephen, P. Gamble, Z. Xie, Y. Yan, Y.-Y. Chen, J. Shin, N. Birenbaum, S. Chung, S. B. Kim, J. Khalifeh, D. V. Harburg, K. Bean, M. Paskett, J. Kim, Z. S. Zohny, S. M. Lee, R. Zhang, K. Luo, B. Ji, A. Banks, H. M. Lee, Y. Huang, W. Z. Ray and J. A. Rogers, *Nat. Med.*, 2018, **24**, 1830–1836.
38 S. Y. Heo, J. Kim, P. Gutruf, A. Banks, P. Wei, R. Pielak, G. Balooch, Y. Shi, H. Araki, D. Rollo, C. Gaede, M. Patel, J. W. Kwak, A. E. Peña-Alcántara, K.-T. Lee, Y. Yun, J. K. Robinson, S. Xu and J. A. Rogers, *Sci. Transl. Med.*, 2018, **10**, eaau1643.
39 C. M. Boutry, L. Beker, Y. Kaizawa, C. Vassos, H. Tran, A. C. Hinckley, R. Pfattner, S. Niu, J. Li, J. Claverie, Z. Wang, J. Chang, P. M. Fox and Z. Bao, *Nat. Biomed. Eng.*, 2019, **3**, 47–57.
40 N. Baït, B. Grassl, C. Derail and A. Benaboura, *Soft Matter*, 2011, **7**, 2025.
41 J.-W. Seo, H. Kim, K. Kim, S. Q. Choi and H. J. Lee, *Adv. Funct. Mater.*, 2018, **28**, 1800802.